Journal of Manufacturing Processes 131 (2024) 604–618

Contents lists available at ScienceDirect

Journal of Manufacturing Processes

journal homepage: www.elsevier.com/locate/manpro

A generalized parametric model for the bonding occurrence prediction in friction stir consolidation of aluminum alloys chips

Riccardo Puleo, Abdul Latif, Giuseppe Ingarao *, Livan Fratini

Department of Engineering, University of Palermo, Viale delle Scienze, Palermo 90128, Italy

ARTICLE INFO

Keywords:
Solid state recycling
Friction Stir Consolidation
F.E.M.
Solid bonding criteria
Aluminum alloys

ABSTRACT

Over the last years solid state processing has been applied as an environmentally friendly recycling method for metal scrap. These approaches, by skipping the melting step, allow substantial energy and resource savings with respect to conventional remelting routes. Specifically, several processes relying on solid bonding phenomenon have been applied to recycle aluminum alloys chips. In this paper, the Friction Stir Consolidation recycling process is considered as solid-state recycling approach to turn chips of three different aluminum alloys namely AA2024, AA6082 and AA5083, into consolidated billet. The paper aims both at validating a new solid bonding criteria specifically designed for Friction Stir Consolidation as well as at proposing a general model to characterize the bonding criterion for each single considered material. In this regard, a correlation analysis and a new parametric model has been developed aiming to understand which material properties were involved in solid bonding occurrence and to predict the bonding limit curve vs temperature by means of material thermo-mechanical properties. The identified criterion and parametric model have been validated by implementing these on the bonding prediction occurrence in Friction Stir Consolidation of AA5083 aluminum chips. Results revealed that just on the basis of some mechanical and thermal properties of the material to be recycled it is possible to identify the threshold for the actual bonding of the material at different temperature levels and, therefore, properly design the recycling process by means of numerical simulation implementation.

1. Introduction

The environmental impact caused by engineering materials production causes almost 25 % of all the anthropogenic emission [1]. Primary aluminum production process is one of the most energy and emissions intensive, making the aluminum production industry responsible for about 3 % of the world's 9.4 Gt of direct industrial CO_2 emissions in 2021 [2]. The main approach for reducing the primary production and decoupling the resource depletion from the economic growth is the implementation of Circular Economy Strategies [3]. The basic idea is to turn process scrap and End-of-Life (EoL) products/components directly into reusable materials or, better yet, into new products/components. Over the last years new processes have been proposed either to recycle process scraps efficiently [4,5] or to reprocess EoL components directly into new component/product [6].

Although several circular economy strategies have been proposed lately (Remanufacturing, Repair, Refurbishment, Reuse, etc.), recycling is the most commonly applied strategy as far as metals are concerned. Despite that, it is worth remarking that for aluminum alloys the conventional recycling route, based on remelting, is neither energy nor resource efficient. Actually, the main drawback for the conventional recycling processes is the permanent material losses occurring during remelting because of the oxidation [7]. In order to overcome such issue, researches have turned to Solid State Recycling (SSR) strategies. These approaches directly turn aluminum scraps into semi-finished products by avoiding the remelting step [8]. The solid-state nature of such process category results in no material losses due to oxidation as well as in a reduced number of intermediate steps to obtain the desired semi-finished product. The solid-state activation depends on pressure, temperature and contact time among surfaces to be joined. Oxides films covering the chips must be broken and dispersed into the metal matrix to allow the metal-to-metal contact. SSR processes, therefore, have to provide the enough temperature and strain to reach the solid bonding conditions among metal chips.

Most of the research in this domain was developed on conventional hot extrusion [9,10] and Equal Channel Angular Pressing (ECAP) [11]. The latter provided better performance as it is characterized by higher strains level allowing solid bonding condition to be fully achieved.

Other recycling processes are characterized, instead, by less strain

* Corresponding author.
E-mail address: giuseppe.ingarao@unipa.it (G. Ingarao).

https://doi.org/10.1016/j.jmapro.2024.09.049
Received 27 April 2024; Received in revised form 5 September 2024; Accepted 12 September 2024
Available online 19 September 2024

Nomenclature

Exp ID	Experimental identification number
FSC	Friction stir consolidation
FSCed	Friction stir consolidation product
p	Normal contact pressure
σ_{mean}	Mean stress
σ_f	Flow stress of the material
$\overline{\varepsilon}$	Equivalent Strain
$\dot{\varepsilon}$	Strain rate
ε_0	Reference strain rate
v	Nodal velocity
w_T	Temperature weight
w_s	Strain weight
Z	Zener – Hollomon parameter
W^{lim}	Threshold limit value/Bonding threshold
W^i	Solid bonding criterion value in the observation loci *i*
r	Correlation coefficient
Gz	Grain size
T_i	Temperature calculated for the i-th calculation step
ε_i	Strain calculated for the i-th calculation step
PP	Plata – Piwnik
PPW	Plata – Piwnik – Weighted
TYS	Tensile yield strength

level such as Spark Plasma Sintering (SPS) processes proposed by Paraskevas et al. in order to consolidate aluminum and magnesium chips [12,13]. However, due to the lack of strain and strain rate occurrence, the consolidation level and final density provided by this process category could not be satisfactory; for these reasons, some authors proposed to apply a further process step after sintering step. Koch et al. [14], propose a process chain made of cold compaction process, a field-assisted sintering (FAST) process and finally a forward rod extrusion process to recycle aluminum alloys chips.

Within SSR process category, friction stir based methods have lately drawn the attention of several researchers. These are the process variants of Friction Stir Welding (FSW) [15]; specifically, the solid bonding mechanics occurring in FSW has been applied for the recycling purposes. In these processes, the friction between chips and tool allows heat generation due to the combined effect of contact pressure and rotational speed of the tool leading to chips welding.

Among them, Friction Stir Extrusion (FSE) and Friction Stir Consolidation (FSC) are the most applied processes for recycling purposes. As far as FSE is concerned, a rotating die is plunged into a cylindrical chamber containing the metal scraps. The stirring action of the tool plastically deforms the materials and forces them into the extrusion chamber [16]. Finally, after densifying and heating, fully dense rods/wires are backward extruded trough an inner channel within the die [17]. Apart from the wire extrusion, some researchers have worked on Share Assisted Processing and Extrusion (ShAPE), where the die configuration enabled the extrudate to push off the mandrel as in conventional extrusion. With ShAPE, chips can be directly converted into tubes and hollow profiles [18,19]. Another continuous process relying on heating due to friction, applied for chips recycling, is the FIRP approach [20]. In this process, chips are fed into the rotating groove of the wheel, which has a continuous rotational movement which transports the particles into the tooling system. Due to the steady reduction of the cross-sectional area of the wheel groove on the basis of the tool insert, the aluminum particles are compacted, heated and plasticized with steady rotation.

The present paper deals with FSC process; it is a discrete production process that turn a chips batch directly into a billet. Actually, a rotating tool is pressed onto chips which are confined in a billet chamber. The heat generated by friction, and plastic deformation results in softening of the material; the interparticle gaps are diminished and then the particles are welded together and consolidated [21]. Actually, this process was first presented by Tang and Reynolds [22]; they obtained solid disks starting from different aluminum alloy chips (2xxx, 5xxx, 6xxx and 7xxx). They revealed a lack of consolidation occurring at the outer bottom part of the disks. Specifically, they assumed that these defects were due to the lower deformation and heat input generated during the process with respect to the upper part of the disk (where the material is directly in contact with the tool). Some of the authors of the present paper proved that the FSCed billet are characterized by non-homogeneous mechanical properties [23], and to address these issues proposed multi-step manufacturing approaches to improve the quality of the consolidation [24].

Because of the non-symmetric nature of the FSC process that can cause a sample characterized by heterogeneous propertied and lack of consolidation, it is essential relaying on numerical models able to support the FSC process design. In this respect, solid bonding prediction criteria implemented on finite element codes can represent powerful tools for the correct engineering of such kind of recycling processes.

Basically, two kind of solid bonding modelling exist: the energy barrier and the film theory formulation. The former approach proposes a threshold value as measure of bonding occurrence; the threshold is calculated by analytical formulations of stresses and/or strains cumulated values. On the other hand, the film theory proposes the concept of oxide film breakage to motivate the solid bonding. In other words, the bonding occurs when the oxide layer covering the material is broken allowing the metal-to-metal surface contact. Actually, over the last years solid bonding criteria formulations integrated with numerical simulation have been implemented for the design of conventional manufacturing processes.

Concerning the energy barrier approach, one of the first implementation was presented by Akeret [25], who defined the critical value as the ratio between the normal pressure and the flow stress of the material evaluated during the process. The first modification of this approach was proposed by Plata and Piwnik [26], they proposed to integrate over time the Akeret model. These first formulations were applied to model the solid bonding occurring in porthole die extrusion process. A further modification of this criterion was proposed by and Donati and Tomesani [27]; they included in the formulation the local velocity to improve the bonding prediction in the dead zones of an extrusion process. Ceretti et al. [28] proved that Plata and Piwnik criterion threshold value decreases with increasing temperature.

The film theory was first investigated by Bay [29] who outlined the main aspect characterizing the solid bonding occurrence: local oxide layers breakage enabling metal micro extrusion that activate material solid bonding. Cooper et al. [30] improved the formulation considering the oxygen captured in the material cavities and applied this approach. Recently, Cooper and Oberhausen [31] have extended the film theory of solid-state welding to consider non-plane strain deformations at the billet-billet interface for modelling the transverse welding in aluminum extrusion.

Concerning the solid bonding criteria specifically developed for chips recycling processes, a very limited number of papers are available in literature. As regards the film theory approach, Kolpak et al. [32] adapted the Cooper and Allwood model [30] to the case of aluminum alloys chips recycling by porthole extrusion process. The model they proposed allowed the quality of the chips bonding to be evaluated with varying geometrical and process parameters. Moreover, the bonding mechanism on port-hole extrusion process was also analyzed by Yu et al.

[33]; in this research, in order to describe the influence of the atomic diffusion, the authors added a modified Arrhenius equation to the already known solid bonding criterion. Based on their consideration, this new version of the Arrhenius equation allows matching the magnitude of the ratio between stresses (σ_m/σ) with the magnitude of the ratio exp(RT/Q). As far as the energy barriers-based approaches, Guley et al. [34], improved the Donati and Tomesani formulation by considering the effect of the shear stress as trigger for the bonding occurrence. The authors identify a shear stress threshold ensuring the oxide layers between chips to be broken. The authors implemented this new approach on porthole die extrusion aluminum alloys chips recycling. Baffari et al. [35], applied conventional Plata and Piwnik criterion to model the bonding of AZ31 magnesium alloy chips when they are processed by Friction Stir Extrusion.

The literature review reveals that although bonding criteria have been analyzed in the last years, their correct formulation depends on the specific process mechanics and, therefore, they are normally adapted to the analyzed process. Also, there is a research need for implementing these approaches on chips recycling processes for a better understanding and modelling of this new process category.

Aware of these research gaps, the authors have recently developed a new solid bonding criterion specifically designed for modelling the bonding in aluminum chips recycling by FSC [36]. In this research the authors proved that the new solid bonding criterion, named Plata – Piwnik – Weighted (PPW), successfully modeled the bonding occurrence in FSC based AA7075 chips recycling. In that paper, the authors supported the effectiveness of the new criterion by showing that conventional criteria (already presented in literature) fail to predict the solid bonding occurrence for FSC recycling.

The present paper aims at strengthening and extending the findings Plata – Piwnik – Weighted criterion; to be more specific, the objective of the present research is twofold.

1/Verifying the effectiveness of the proposed criterion on different aluminum alloys. In this regard, the entire methodology set up in the previous research, is here applied on two new aluminum alloys, namely AA2024 and AA6082. The idea is to test the flexibility of the proposed approach to make the findings concerning the effectiveness of the PPW criterion more general.

2/Proposing a modelling effort relying on the data obtained on three different materials. The aim is the identification of a parametric model able to describe, with a single analytical expression, the bonding occurrence of different materials. In this respect, a correlation analysis was carried out to identify the material properties that actually affect the solid bonding limit curve of a given material. A parametric model was proposed to generalize the trend of the bonding limit curve vs temperature by means of specific thermo-mechanical properties of the materials. The developed model was validated on a further (fourth) aluminum alloy: AA5083.

The structure of the paper consists of 7 main sections: in Section 2 the procedure for the experimental and numerical campaign was reported; in Section 3 the solid bonding criteria used to evaluate the bonding occurrence are shown. The methodology and the results are described in Section 4 while the new parametric modelling is discussed in Section 5; in Section 6 the validation of the new procedure is presented. The main findings are summarized in Section 7.

2. Materials and methods

In this section, the experimental and numerical procedure are explained. Specifically, the study presented in this paper involves two main parts: an experimental campaign which provided the data used to develop the experimental criterion and a numerical campaign that was carried out to study the performance of the solid bonding criteria through an image correlation analysis in MATLAB environment.

2.1. Experimental campaign

The experimental campaign of the present research is the extended investigation of the previous study, developed only on the AA7075 [36]. The chips of three different aluminum alloys, AA2024-T4, AA6082-T6, and AA5083-H111, were utilized. These chips were obtained from the as-received materials, with details listed in Table 1, by using milling operation with a tool rotational speed of 1250 rpm, a feed rate of 28 mm/min and a cutting depth of 1 mm. The choice of these materials was driven by the difference in their thermo-mechanical properties, aiming to gain deeper insights into FSC process mechanics. Further, AA2xxx, AA5xxx, and AA6xxx alloys are popular materials in aerospace, marine, and automotive applications, respectively [37].

The used experimental setup consisted of ESAB LEGIO, a dedicated friction welding machine with 35 kN vertical load maximum capacity. A tool of H13 steel with 25 mm nominal diameter was coupled to head of ESAB machine and a H13 steel cylinder die with 25 mm was integrated onto the working table (shown in Fig. 1). The chips were first cleaned and then dried after the machining process. The cleaning step was performed by submerging them in acetone for 30 min. Then a fixed mass of 15 g cleaned chips was loaded inside the die chamber and compacted with 5 kN load in order to avoid sprinkling out of the chips during consolidation stage. After the pre-compaction, the tool rotation was activated with pressing load initiating from 5 kN. The load was constantly increased from 5 kN to 20 kN with 0.5 kN/s step increment during the first 30 s. This step was termed to as transition phase. Here it is important to note that due to available machine limitations, an instant load achievement of 20 kN was not possible for the sake of machine safety. Consequently, a mandatory transition period of 30 s preceded the consolidation step. Productive time commenced upon reaching a force of 20 kN, and the duration subsequent to achieving 20 kN was termed as the consolidation time. Finally, chips were consolidated with load of 20 kN at different rotational speed and processing time. The experimental plan shown in Table 2 was executed for AA2024-T4 and AA6082-T6. For these materials, four experiments (Exp 1 to Exp 4 of Table 2) were performed to analyze and model the bonding occurrence; one experiment, with different process parameters setting (Exp 5), was used to validate the results. To verify the new introduced formulation based on the here proposed linear parametric model (described in Section 5), FSC recycled billets were manufactured from a fourth, new, material (AA5083-H111); for this material only Exp 1 and Exp 4 were developed as it was used for validation purposes.

It is worth remarking that, the choice of parameters was driven by several reasons; the authors proved that with the ESAB LEGIO machine used in this research, the process window is quite limited as discussed in [38]. To be more specific, a further increase in rotational speed and processing time beyond a given threshold does not provide any actual improvement. Secondly, to draw a comparison among different aluminum alloys consolidation, it was important to adopt a uniform set of process conditions, as those employed by the authors during FSC of AA7075 billets [36]. Additionally, the selected process parameters conditions allow the production of aluminum alloy billets with substantial different levels of consolidation quality; the latter aspect is crucial for predicting bonding quality across a wide range of process

Table 1
Details of as-received materials.

S#	As-material	As-shape	Vickers hardness [Hv]	Grain size [μm]	TC [W/mm K]	SHC [J/g °C]
1	AA2024-T4	Extruded round bar	100	52.2	0.13	0.96
2	AA6082-T6	Extruded angle bar	98.7	8.6	0.17	0.9
3	AA5083-H111	Rolled sheet	70	75	0.12	0.87

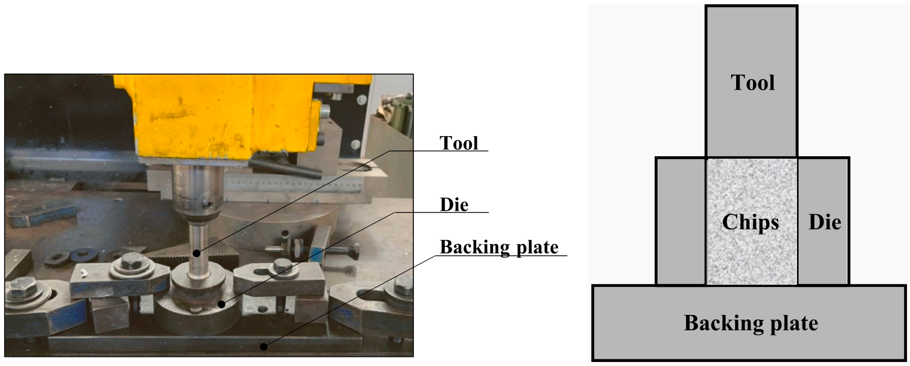

Fig. 1. Friction stir consolidation experimental setup and process sketch.

Table 2
Process parameters setting of the developed FSC tests.

Exp ID	Rotational speed [RPM]	Mass [g]	Transition period [s]	Consolidation time [s]
Exp 1	1500	15	30	0
Exp 2	1500	15	30	10
Exp 3	1500	15	30	20
Exp 4	1500	15	30	30
Exp 5	1000	15	30	20

conditions [36].

For each sample, hardness and microstructure characterization were developed; The samples were, therefore, first sectioned by using a grinding wheel with low cutting speed and polished. Then, the samples were etched using Keller's reagent (0.5 ml HF, 1.5 ml HCl, 2.5 ml HNO_3, and 95.5 ml H_2O). GX51 Olympus optical microscope was utilized to analyze the microstructure by using 5× and 50× lenses. The grain size was measured throughout the billet section at 119 observation loci equally spaced at a distance of 1.5 mm (Fig. 4). The method of intercepting in accordance with the ASTM E112–96 standard test was used by utilizing ImageJ software. The same observation loci were also analyzed for the hardness test. The hardness was measured through the Vickers hardness (Hv) test by applying Hv5 load in accordance with ISO 6507 standard. A load of 49 N (5 kg) was applied for 15 s. These analyses are needed for the definition of the experimental bonding criterion (see Section 4.1). This criterion allows the bonding occurrence in the FSCed billet to be described, and it is based on hardness and grain size values.

2.2. *Numerical campaign*

The FSC process simulation was performed using the commercial software SFTC DEFORM 3D™. Specifically, the model consists of four components: tool, die, backing plate and chips (Fig. 2). The tool, as well as the die and the backing plate, was considered as a H-13 steel rigid component characterized by a mesh size of 30,000 elements. A friction shear factor equal to 0.2, 0.25 and 0.28 were used to model the tool-chips contact for AA2024, AA6082 and AA5083, respectively. On the other hand, the chips were considered as a porous billet, using the Shima and Oyane [39] formulation to model the discrete nature of the starting billet. An initial relative density value of 0.44 was used to model the starting billet porosity; this value was experimentally quantified. The

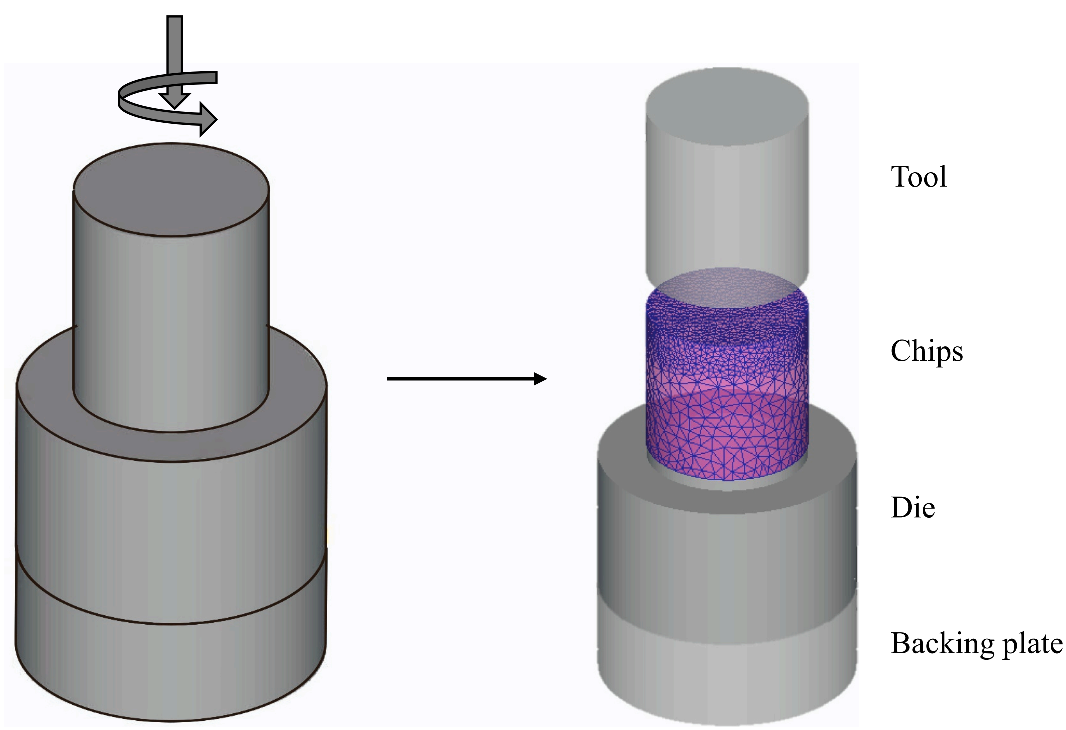

Fig. 2. Numerical model for tool, die, backing plate and porous billet.

heat transfer coefficient was considered equal to 11 W/mm/K, this value was selected according to what reported in [40], where a numerical approach was used for simulation friction stir welding processes. The good matching between the numerical and experimental temperature trends at the bottom of the billet (see Fig. 3) prove the effectiveness of the selected value. A mesh of 30,000 elements were used for the billet; a refining mesh window was also located in the tool-billet contact surface. The material mechanical behavior was evaluated though the study of the ASM compendium and the database JMatPro, for each material. The temperature stress-strain-strain rate curves obtained for AA2024, AA6082 and AA5083 are shown in Eqs. (1), (2) and (3), respectively.

$$\sigma_f = 8.958 \bullet (18486.1 + \bar{\varepsilon})^{0.1729} \bullet \dot{\varepsilon}^{0.0485} \bullet exp^{549.865/T} \quad (1)$$

$$\sigma_f = 0.563 \bullet (34.819 + \bar{\varepsilon})^{1.49} \bullet \dot{\varepsilon}^{0.405} \bullet exp^{916.48/T} \quad (2)$$

$$\sigma_f = 6.4963 \bullet (18.546 + \bar{\varepsilon})^{0.1030} \bullet \dot{\varepsilon}^{0.00404} \bullet exp^{1090.52/T} \quad (3)$$

The numerical simulation was tuned and validated through experimental temperature measurement at the center bottom of the billet by using a K-thermocouple. In Fig. 3 temperature trends obtained from the experimental and numerical measurement for each material are reported; a good overlapping can be observed.

The aim of these simulations was the acquisition of all the stress and strain values characterizing the FSC over the processing time (transition and consolidation). The trends of such variables allow different bonding approaches to be analyzed and the bonding occurrence in FSC better investigated.

3. Analyzed bonding criteria

As mentioned in the introduction, the existing bonding criteria can be divided into two categories: energy barrier theory criteria and film theory criteria. The authors have proved that the available film theory model [32] fails in modelling the bonding occurrence in FSC process and, moreover, they are very complex to be implemented as they require several assumptions to be made and coefficients values to be identified. For these reasons, only the energy barrier bonding criteria are analyzed, specifically the formulations reported in Table 3 will be taken into account. Along with the criteria reported in Table 3, the authors have tested other criteria based on the energy barriers theory [33,34]; since no relevant changes, both in terms of theoretical formulation and in the related obtained results, were observed, the discussion is limited to those reported in Table 3 for the sake of clarity of presentation.

The first three criteria were already available in literature and were used to predict the bonding occurrence in extrusion processes. The last two criteria of Table 3, instead, were designed by the authors for the FSC process. All the criteria here reported were tested for each analyzed material by identifying the thresholds with an iterative procedure reported in Section 4.2.

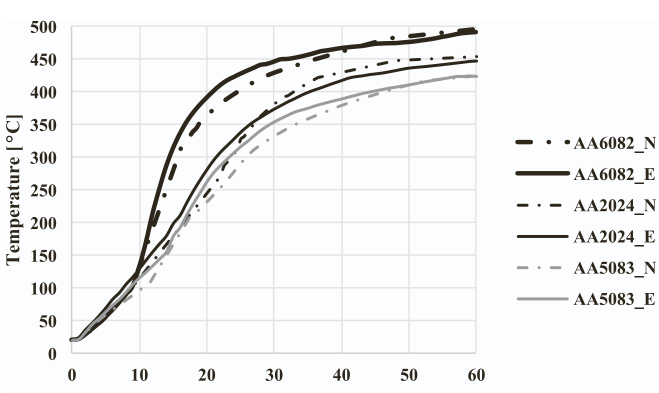

Fig. 3. Comparison between experimental and numerical temperature profiles during FSC, at center bottom of the billet (N = numerical, E = experimental).

Specifically, the Plata – Piwnik – Weighted (PPW) criterion improves the concept of Plata – Piwnik (PP) by adding two weights related to the temperature and strain (w_T and w_s). These weights have the effect of reducing the count of the integer on time where the temperature and/or strain impact is lower; the equations of w_T and w_s are shown in Eq. (4).

$$w_T = \frac{T_i - T_{i-1}}{T_i} = \frac{\Delta T}{T_i} \; w_s = \frac{\varepsilon_i - \varepsilon_{i-1}}{\varepsilon_i} = \frac{\Delta \varepsilon}{\varepsilon_i} \quad (4)$$

The second formulation proposed by authors concerns the use of the Zener-Hollomon parameter (Eq. (5)) to link the Plata – Piwnik criterion to the recrystallization phenomenon. This criterion was applied considering a temperature activation threshold (480 °C); this temperature threshold was identified with an iterative approach in order to optimize the matching between the experimental results and the predicted ones obtained with the adopted solid boning criterion (the procedure was implemented on all the experiments from Exp 1 to Exp 4).

$$Z = \dot{\varepsilon}\, exp^{\left(Q/R \bullet T\right)} \quad (5)$$

where R is the gas constant (8.314 J/mol K), T is the temperature (K) of the point and Q (J/mol) is the activation energy (AA2024 [41], AA6082 [42] and AA5083 [43]).

4. Discussion of the results

In this section, the obtained experimental and numerical bonding maps are analyzed for the AA2024 and AA6082. The obtained results will be compared to those already obtained for the AA7075. The objective is to strengthen the effectiveness of the Plata - Piwnik – Weighted criterion with respect to other criteria in FSC bonding occurrence prediction.

4.1. Experimental bonding criterion

The aim of the experimental campaign is the definition of the experimental bonding map for each Exp I.D. (1 to 4) reported in Table 2 and for each of the analyzed material. The experimental bonding map derives from the definition of an experimental bonding criterion defined in [36] as follows:

> "The bonding occurs when grain size and hardness value exceed simultaneously the threshold of 2 μm and 60 % of base material hardness, respectively. This means that when the grain size and hardness value of an observed locus are greater than 2 μm and 60 % of base material hardness, it can be considered as consolidated."

The microstructural view of Exp 1 and Exp 4 for the AA2024 can be seen in Figs. 5 and 6 while those of AA6082 are reported in Figs. 7 and 8. To better highlight the grain size evolution, only the Exp 1 and Exp 4 are shown as represent the first and the last time acquisition.

It is clearly visible from Figs. 5–8 a direct correlation between processing time and the consolidation effect. The increasing processing time leads to an increase in the consolidation effect throughout the observed section of the specimen. In particular, for Exp 1 of AA2024 material (Fig. 5) the upper section of the billet was fully recrystallized, but an unconsolidated zone with loose bonding chips was noticed at the bottom section of it. Further, the microstructure of the bottom zone was not much altered compared to the starting input material (chips). It indicates that processing time was not enough to achieve full consolidation. As the processing time increased to 60s in the case of Exp 4 (see Fig. 6), the consolidated zone expanded towards the bottom resulting in a more consolidated area with good bonding conditions among the chips except near the external surface at the bottom. This zone, which can be

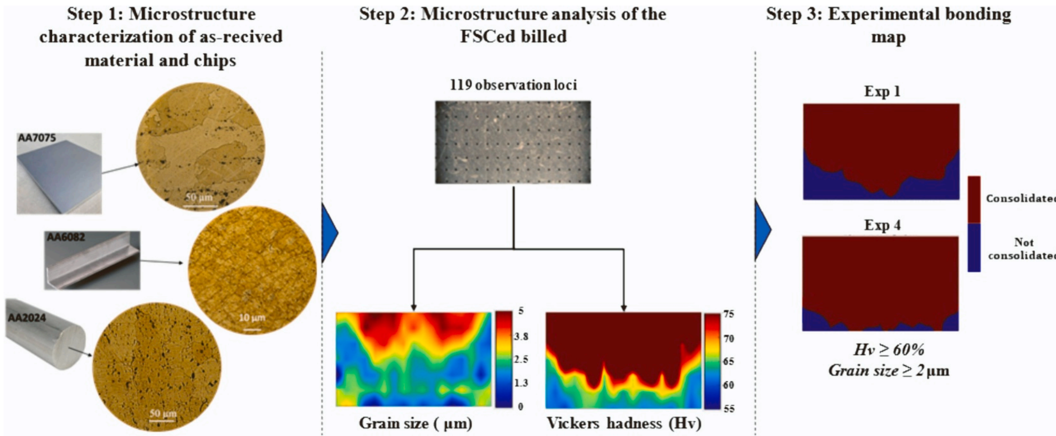

Fig. 4. Procedure adopted for the experimental campaign.

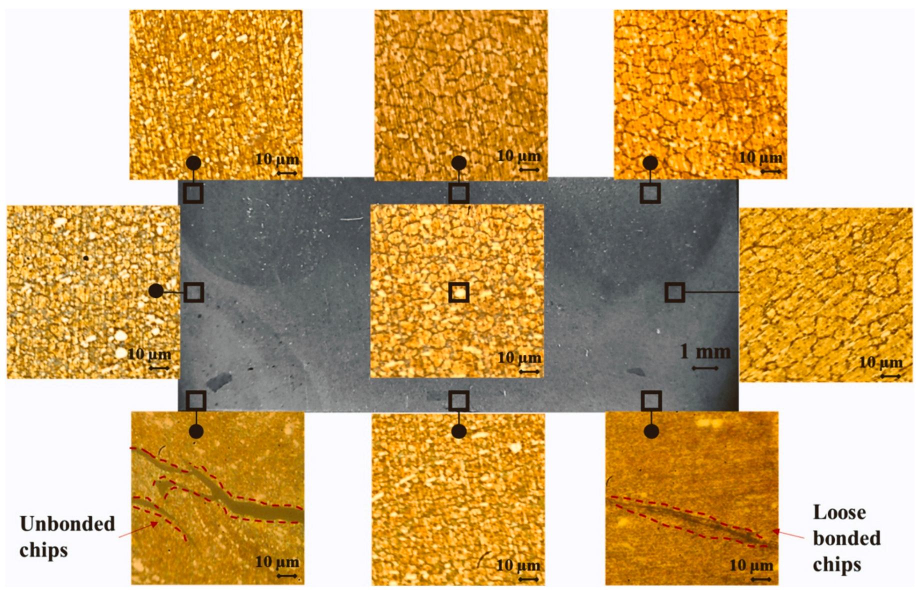

Fig. 5. Microstructural view of the grains for AA2024, Exp. 1.

compared to the dead zone of extrusion process, can never reach the consolidation conditions irrespective of the processing conditions [22].

Increasing processing time processing led to a larger consolidated area with improved billet quality in the case of the AA6082 (comparing Figs. 7 and 8). Concerning the influence of material, thermophysical characteristics such as the thermal conductivity of the input material, could be assumed to also play an important role. A material with a higher thermal conductivity proves conducive in transferring heat from rotating towards the bottom section. Therefore, a higher heat transfer rate leads to a change in the microstructure of the bottom more rapidly compared to a material characterized by a lower value of thermal conductivity as can be seen in the case of AA6082 compared to AA2024 (comparing Figs. 5 and 7). On the other hand the AA6082 micrography show that the grain growth is limited to the upper half part of the billet's cross section.

However, a clearer visualization of the bonding map can be obtained by analyzing the hardness and grain size values and combing them by the defined experimental bonding criterion. The grain size and hardness distributions for AA6082 along with the derived experimental bonding map are reported in Fig. 9. The evolution of the consolidated area is clearly visible as it expands bottomward from Exp 1 to 4. It is possible to notice, that for the AA6082 a large part of the billet is still not consolidated even in Exp 4. For the sake of clarity of results presentation, the grain size, hardness distributions and related experimental bonding map of Exp 1 to Exp 4 for the AA2024 are not reported. However, it is worth mentioning that for the case of AA 2024 an almost fully consolidated billet can be obtained when process conditions of EXP 4 are obtained.

Overall, the consolidation region increases with increasing processing time; this phenomenon is due to the non-symmetric nature of the process, as the strain and heat flow start from the top region and move downwards. This finding has been already discussed by Xi et al. [21] Latif et al. [24].

4.2. Numerical bonding maps

The obtained experimental bonding maps were used as benchmark for the tuning and validation of the solid bonding criteria listed in Table 3. Specifically, for each criterion the related thresholds value will be identified for each Exp I.D. This value must guarantee the best overlapping between the predicted numerical bonding map and the experimental one. For the correct identification of these thresholds, the procedure made of the following steps was implemented:

Step 1: Numerical and experimental test development.

Step 2: Numerical and experimental data collection.

Step 3: Definition of the experimental bonding criterion and calculation of solid bonding map for each Exp I.D.

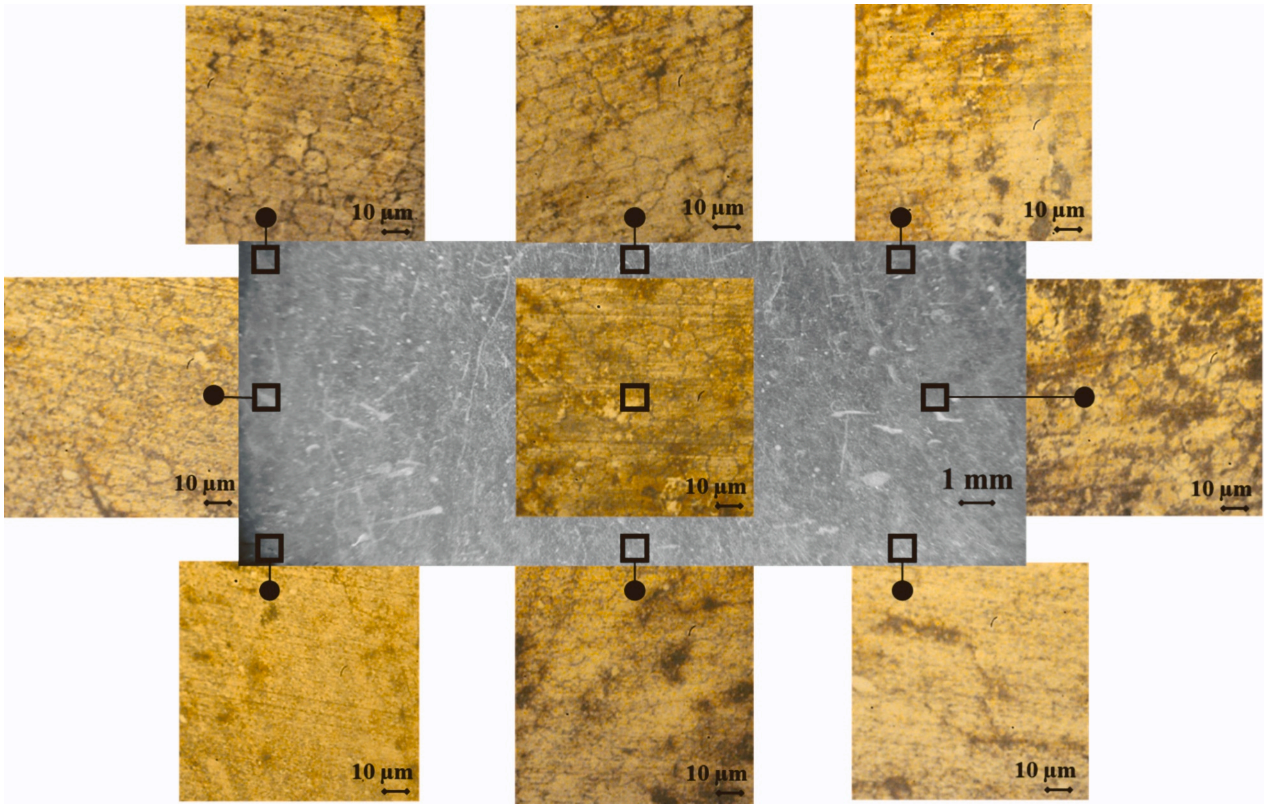

Fig. 6. Microstructural view of the grains for AA2024, Exp. 4.

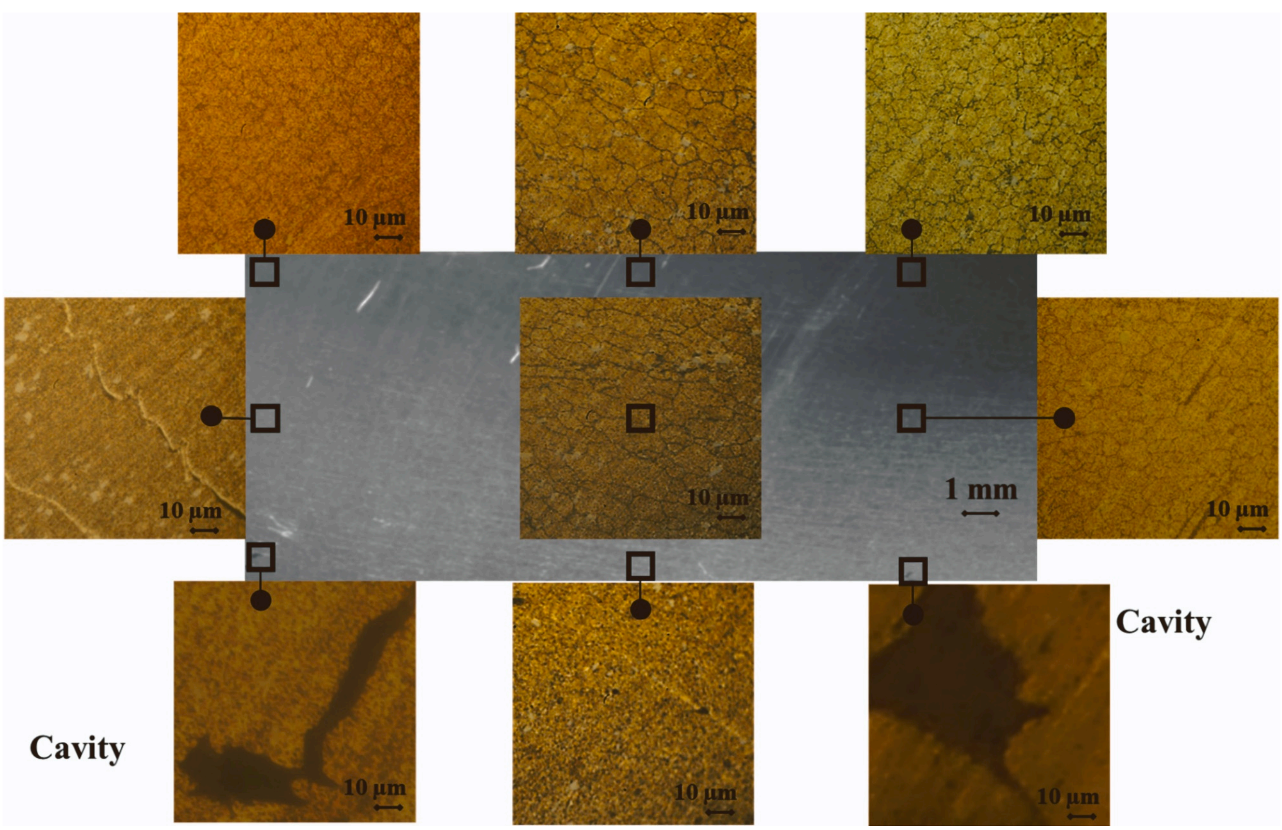

Fig. 7. Microstructural view of the grains for AA6082, Exp. 1.

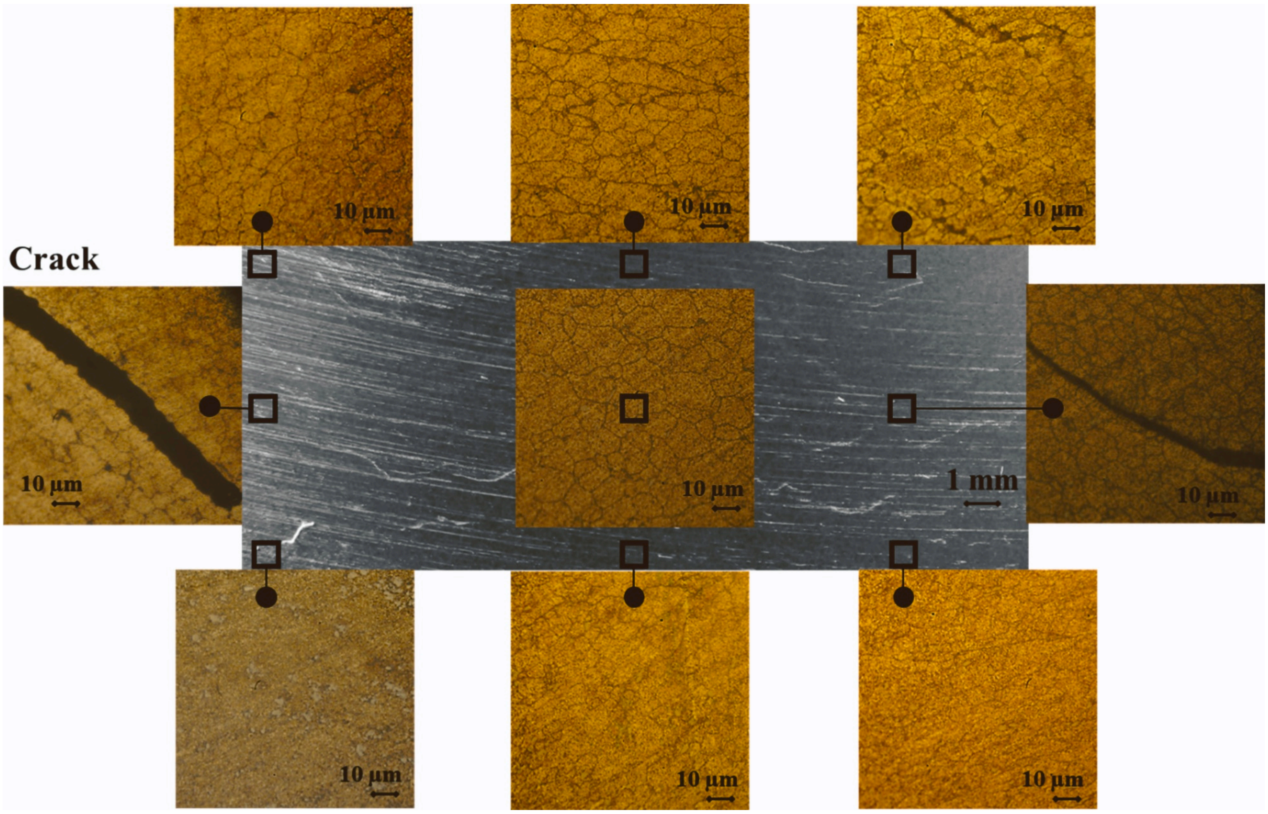

Fig. 8. Microstructural view of the grains for AA6082, Exp. 4.

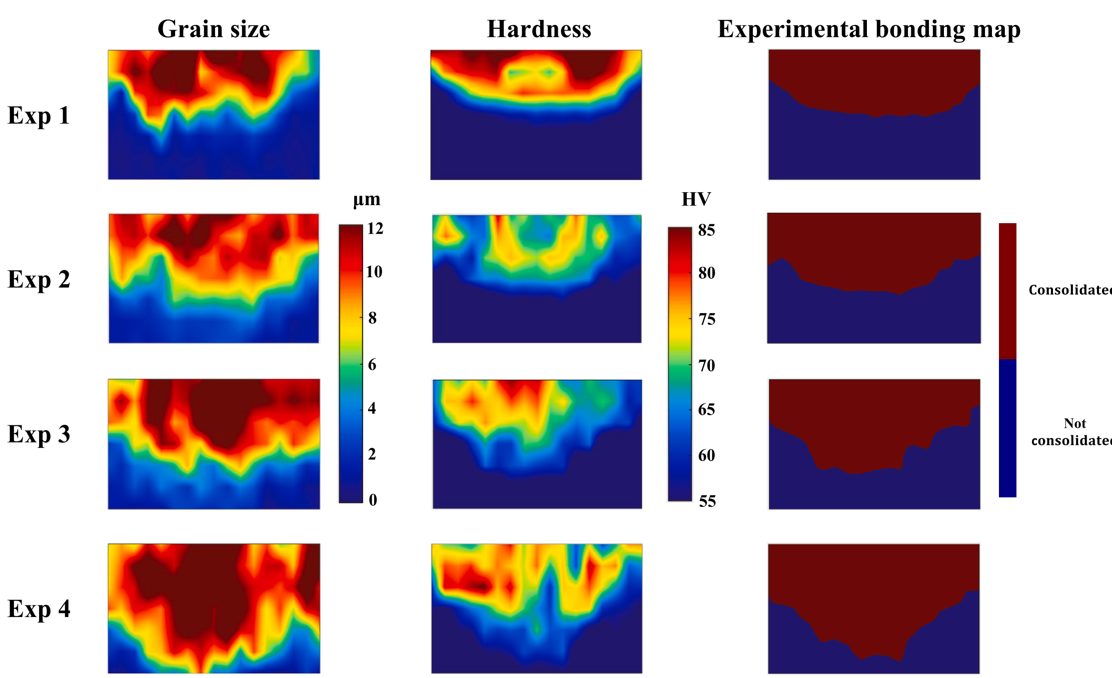

Fig. 9. Grain size and hardness distributions and experimental bonding map for Exp 1 to Exp 4 (AA6082).

Step 4: Iterative calculation using an image comparison model using MATLAB environment aimed at the identification of the proper W^{lim} value.

Step 5: Solid bonding threshold identification (W^{lim}).

Since the performance of each criterion was widely described in the previous analysis [36] for the AA7075 and since similar results were obtained for the new aluminum alloys here analyzed, the results are here discussed only commenting on the results provided by the Plata – Piwnik (PP) and the Plata – Piwnik Weighted (PPW) criteria. The numerical and the experimental bonding maps for AA2024 is reported in Fig. 10.

In this study the performances were evaluated through an image comparison; the dark red area of the solid bonding criteria map,

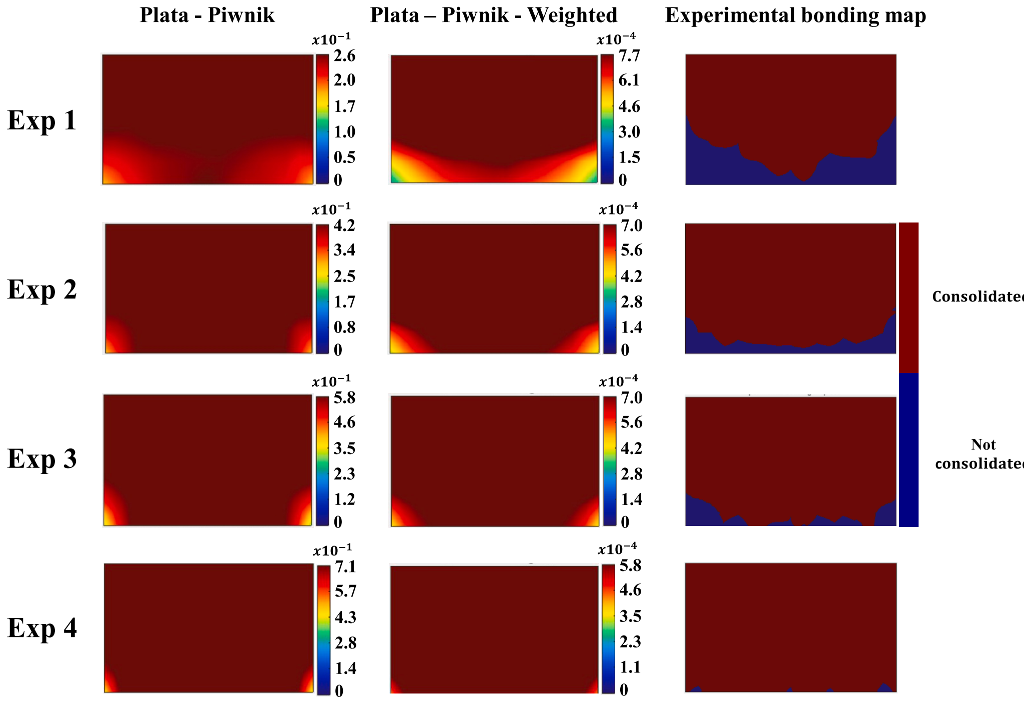

Fig. 10. Calculated solid bonding maps and the experimental bonding maps (AA2024).

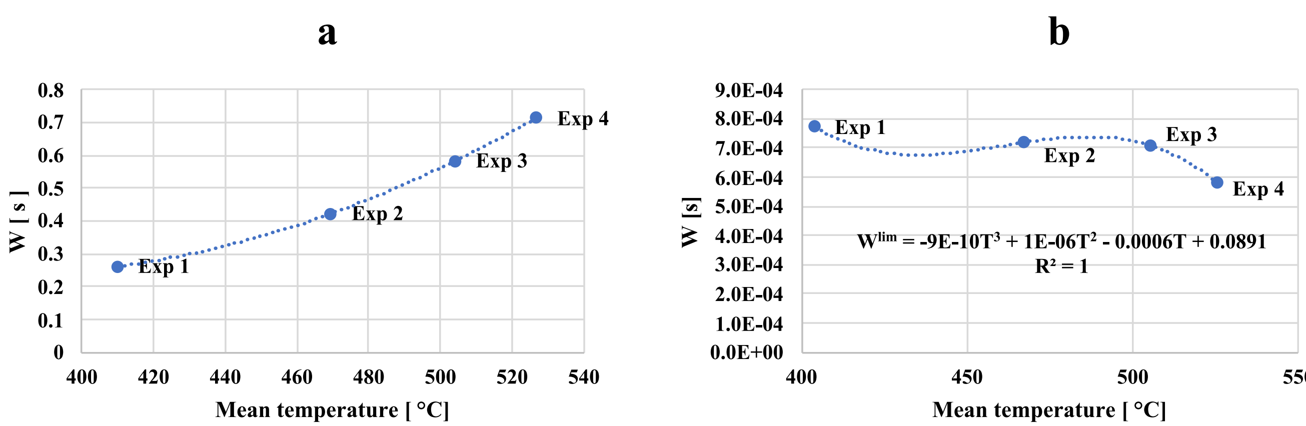

Fig. 11. Example of AA2024 W^{lim} (threshold) temperature trends for the PP (a) criterion and for the PPW (b).

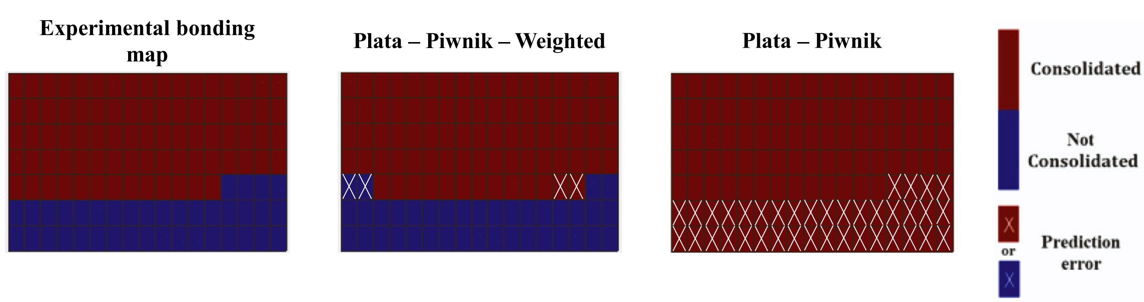

Fig. 12. Graphical analysis of the error's prediction for the validation test, case study AA2024.

representing the material that exceeds the threshold and can be considered as consolidated, was compared to the dark red area of the experimental bonding map which represent the real consolidated zone. The matching level between the experimental and numerical surfaces was quantified in terms of "correlation coefficient" as described in [36]; the correlation coefficients obtained for all the tested criteria together with the identified thresholds values are reported in Table 4. It is possible to notice that Donati – Tomesani [27] and PPW [36] criteria provide the best performance and, overall, with increasing the processing time the prediction performance of each criterion improves. The

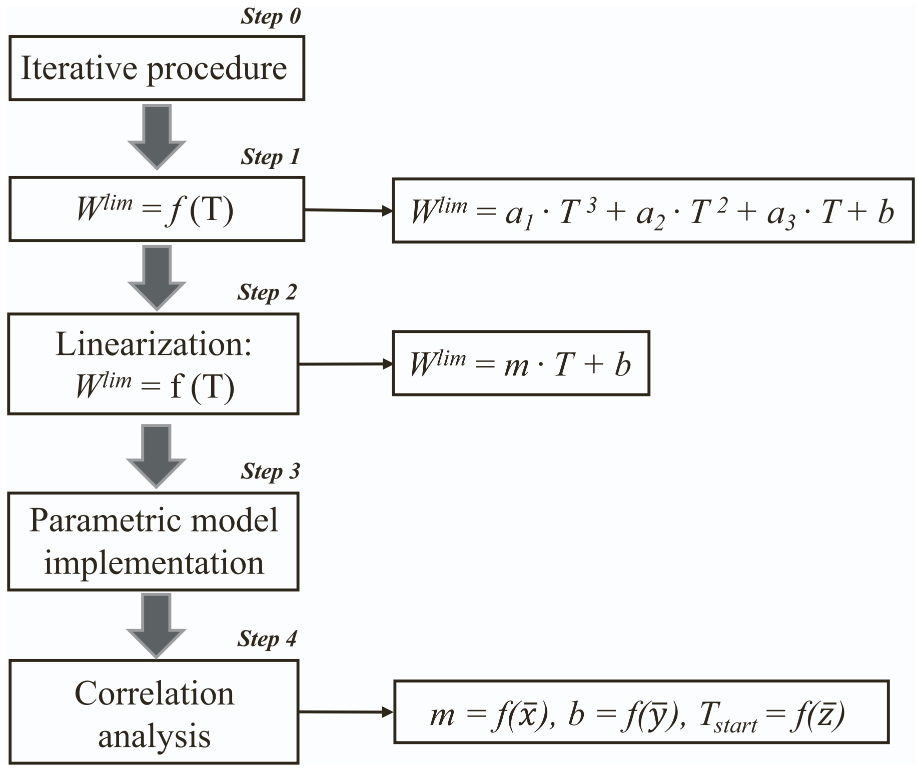

Fig. 13. Workflow for the parametrization of the bonding limit curve, where *a* is the constant values (third-order curve), *m* and *b* are the slope and the y-intercept of the straight line, respectively.

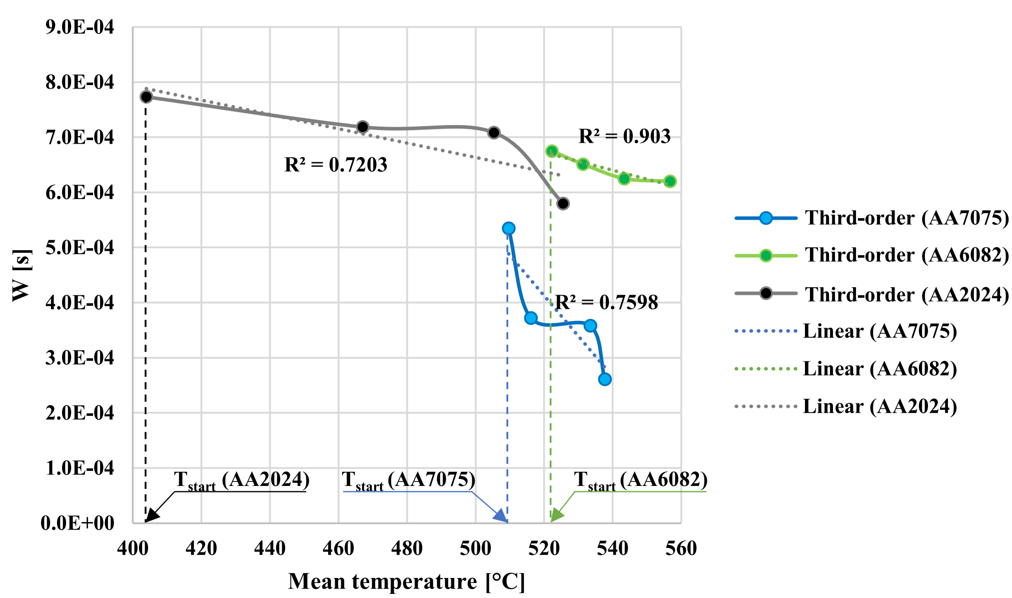

Fig. 14. W^{lim} vs mean temperature curve evaluated in four observation windows (points) for three materials. Exp 1 up to Exp 4 from left to right (for all the three curves).

results are satisfactory as the numerical bonding maps perfectly mimic the experimental ones, as it is possible to notice in Fig. 10.

Actually, for the AA2024 alloy case both the PP and PPW criterion have good performance, proved by both the correlation coefficient values of Table 4 and the maps of Fig. 10. Despite that, it is worth mentioning the W^{lim} values increase moving from Exp 1 to Exp 4 for most of the criteria reported in Table 4; it means that W^{lim} increases with increasing the processing temperature. Specifically, this trend can be seen in Fig. 11 where PP and PPW W^{lim} values obtained for each EXP I.D. are plotted.

This trend cannot be considered a reliable result if the solid bonding mechanics is considered: as a matter of fact, higher temperature increases the material softening effect making easier the sold bonding condition achievement; the bonding limit must, therefore, decrease with increasing the temperature [28]. Actually, the only criterion showing a clear decreasing trend with increasing temperature is the PPW recently presented by the authors.

Table 4 lists also the results obtained for the T for AA6082. The

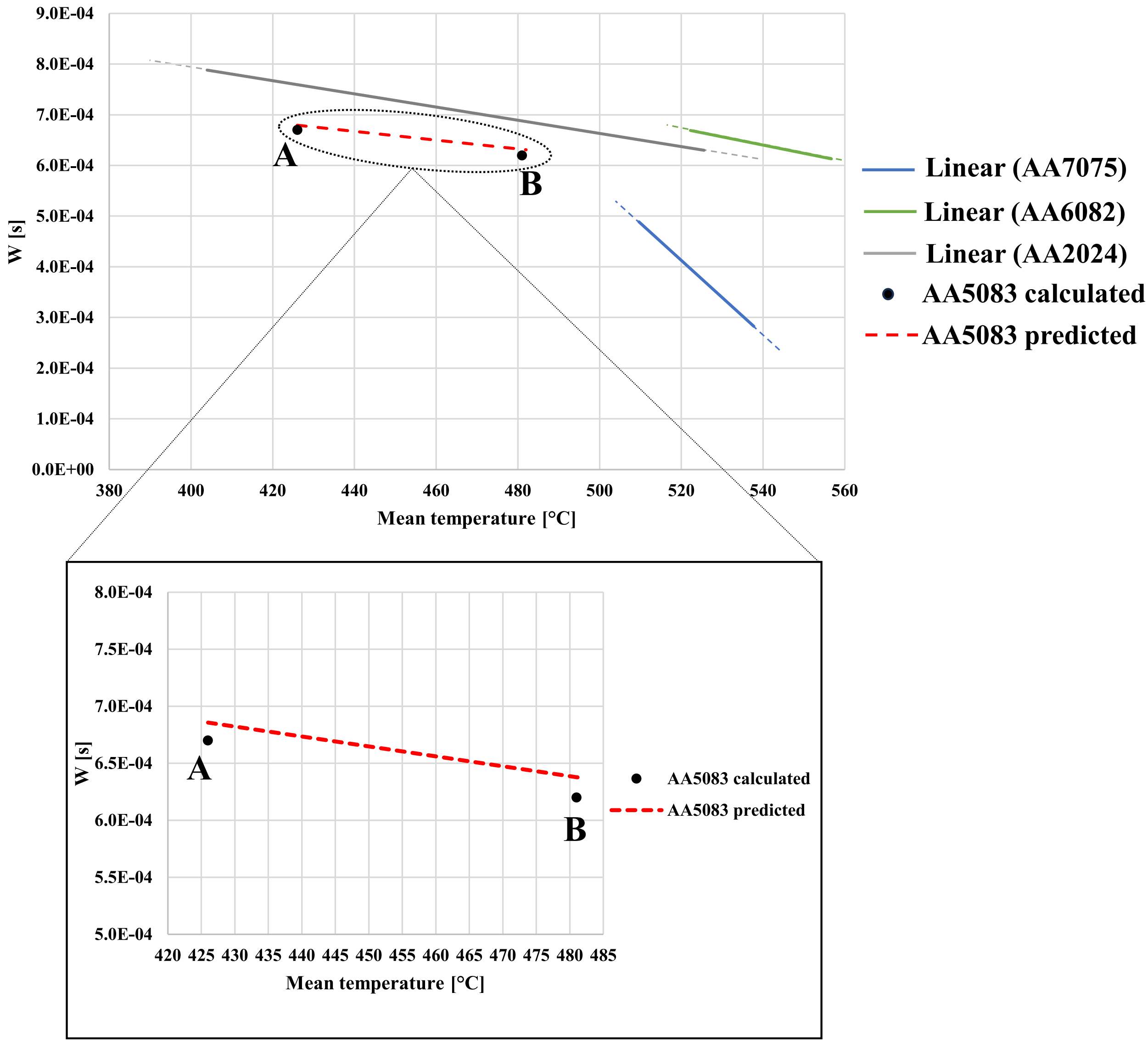

Fig. 15. W^{lim} linear models.

Akeret and PP criteria provide poor results in terms of correlation coefficient, on the other hand the PPW criterion is the only criterion providing a clear decreasing W^{lim} trend with increasing temperature is the PPW.

In order to validate the performance of the proposed criterion on these two new aluminum alloys here tested, one more experiment for each alloy was performed. Specifically, the used process parameters are the Exp 5 configuration reported in Table 2. It is worth remarking that although the Exp 5 is characterized by the same process condition as EXP 3 apart from a reduced rotational speed, the obtained bonding area is definitely different to those characterizing Exp 1 to Exp 4. Actually, the authors have proved that a reduced rotational speed leads to both a reduction in processing temperature and strain and strain rate levels. Therefore, the bonding occurrence is strongly affected by this process parameter variation.

The validation procedure is based on the comparison between the predicted bonding map and the experimental bonding map generated by acquiring the hardness and grain size values (see Section 4.1) for EXP 5 test. For each criterion the W^{lim} vs temperature values were interpolated by a third order model (see Fig. 11b), this model allows the W^{lim} for a given processing temperature to be quantified. By performing the numerical simulation in Exp 5 conditions, it was possible to acquire stress, strains and temperature values for solid bonding criterion values (W^i) calculation in each of the 119 observation loci. After that, it was possible to calculate the W^{lim} for each locus by applying the third order model as the one reported in Fig. 11b by using only the local temperature value as input parameter. The numerical bonding map was, therefore, carried out by performing local solid bonding criterion values comparisons: if the W^i value is higher than the calculated W^{lim}, that point was labeled as consolidated, vice versa it was labeled as not consolidated. Finally, the consolidated/not consolidate map resulting from this analysis was compared with the experimental bonding map.

The validation results for the AA2024 are reported in Fig. 12 where the predicted numerical bonding map by the PPW and the PP criteria are reported along with the experimental bonding map. In order to improve the results visualization each observation loci are represented by a small rectangle (red = consolidated; blue = not consolidated). It is possible to note that the PPW criterion has an excellent prediction performance as it mistakenly predicts the bonding occurrence only in 4 loci. Whereas the PP provides poor performance overestimating the bonding map extension. This means that, although PP criterion has good correlation coefficients (at least for the AA2024), it cannot predict the bonding occurrence for conditions different from those the cubic model was built on; in other words, it cannot be used as a predicting criterion. The

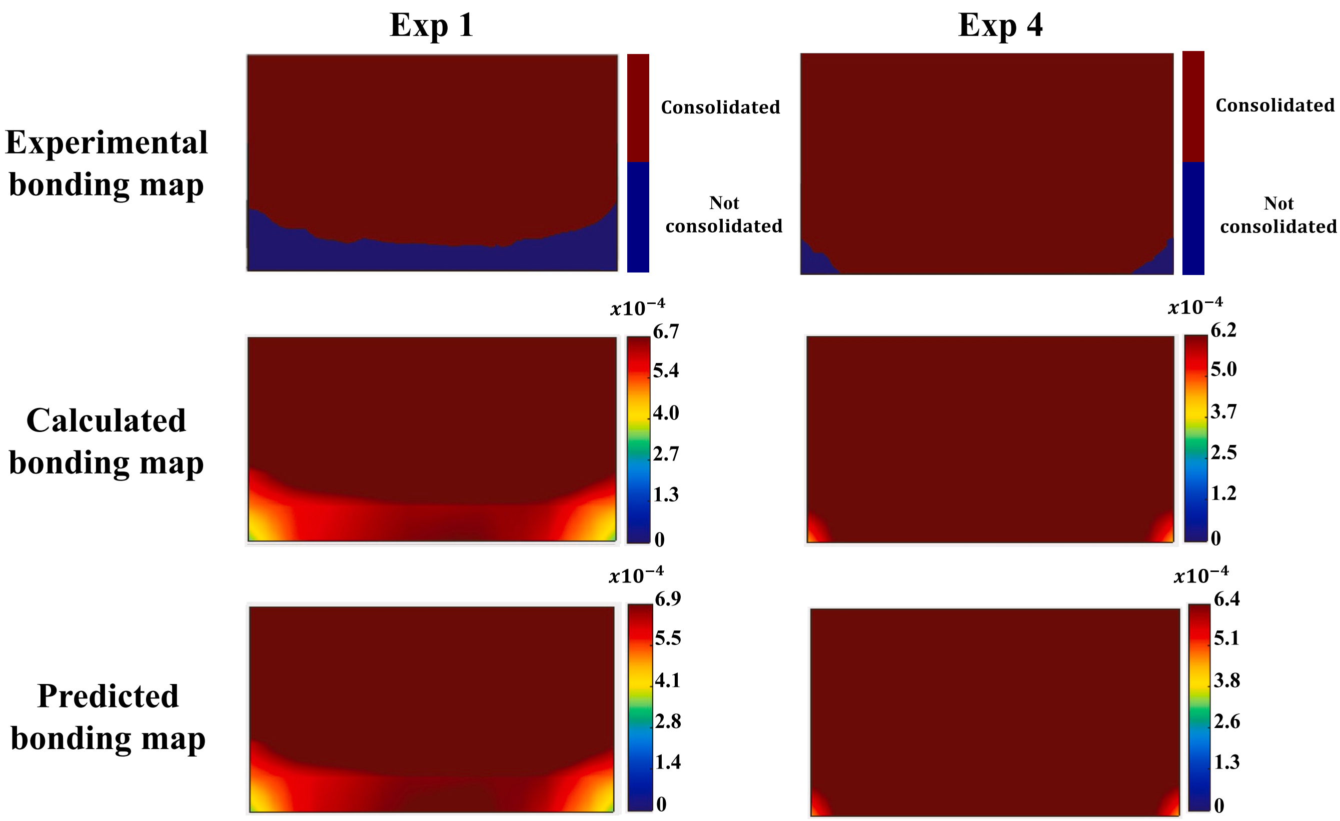

Fig. 16. Experimental, calculated and predicted bonding maps for AA5083 in EXP 1 and EXP 4 conditions.

Table 3
Solid bonding criteria analyzed for modelling the FSC bonding occurrence.

Criterion	Equation
Akeret [25]	$W_1 = \frac{p}{\sigma_f}$
Plata and Piwnik [26]	$W_2 = \int \frac{p}{\sigma_f} dt$
Donati and Tomesani [27]	$W_3 = \int \frac{p}{\sigma_f} dt \bullet v$
Plata - Piwnik – Weighted [36]	$W_4 = w_t \bullet w_s \bullet \int \frac{\lvert\sigma_{mean}\rvert}{\sigma_f} dt$
Plata - Piwnik – Zener [36]	$W_5 = \begin{cases} 0, & T < 480^\circ C \\ \int \frac{\lvert\sigma_{mean}\rvert}{\sigma_f} \bullet \frac{1}{z} dt, & T \geq 480^\circ C \end{cases}$

Note: Plata – Piwnik [s], Donati - Tomesani [mm], Plata – Piwnik – Weighted [s], Plata - Piwnik – Zener [s^2].

authors believe that the knowledge generalization capacity of a given criterion is strongly related to the appropriateness of the W^{lim} trend versus temperature.

The results of the validation procedure for each criterion are reported in Table 5 for AA2024 and AA6082. It is possible to see that the best performance in predicting the bonding occurrence in FSC are provided by the PPW. In fact, the percentage of loci mistakenly predicted is equal to 4 % for AA2024 and 9 % for AA6082. Good performance is provided also by Donati and Tomesani criterion.

These results allow to positively answer to the first question of the present research. Actually, it has been proved that the criterion designed by the authors is effective on different aluminum alloys. Specifically, it allows predicting and modelling the bonding occurrence in FSC processes correctly; the provided performances are better than those provided by the other criteria. This criterion particularly outperforms the other criteria in generalization capability, in fact provide the best performance in the validation test.

5. Model generalization - linear parametric model development

In this section, a parametric model is presented with the purpose to generalize the bonding limit curve by means of a predictive parametric linear model based on the thermo-mechanical material properties. The choice of shifting towards a linear model was driven by the will to simplify the modelling effort, keeping up the bonding prediction performance of the model itself. The parametric model was developed following the workflow reported in Fig. 13.

In the modelling, the results obtained with the PPW criterion were used for the three different materials. The trends of W^{lim} values vs temperature, instead of being interpolated by a third order polynomial curve, were approximated by linear models. The cubic and linear curves for all the analyzed materials are reported in Fig. 14.

In order to test the prediction performance of the linear model with respect to those of the cubic model, a performance check step was executed. The performance check was developed by comparing the bonding prediction accuracy provided either by the cubic or by the linear models with the experimental bonding map. Results in terms of correctly predicted loci are reported in Table 6. As it is possible to note, by using the linear model only a slight worsening in prediction accuracy occurs, this result makes the linear models reliable tools for the modelling of solid bonding occurrence in FSC.

It should be observed that in Fig. 14 for each material a T_{start} temperature is indicated, namely a temperature threshold at which bonding phenomenon is firstly recognized.

Once the linear models were obtained, it was possible to focus on the parametric model development. Specifically, the idea was to express the slope (*m*), the y-intercept (*b*) and the starting temperature (T_{start}) as a function of the thermo-mechanical properties of the analyzed material. In this regard, the properties reported in Table 7 were taken into account. In this table the identified m, b and T_{start} values for the three different materials are also reported. Tensile tests were developed on the base materials to obtain UTS, TYS and EB values; thermal properties

Table 4
W^{lim} and correlation coefficient for both criteria, case study AA2024 and AA6082.

Criterion	Exp ID	AA2024		AA6082	
		Correlation coefficient	W^{lim}	Correlation coefficient	W^{lim}
Akeret (1992)	Exp 1	71 %	$1.7 \cdot 10^{-1}$	67 %	$3.4 \cdot 10^{-1}$
	Exp 2	81 %	$1.9 \cdot 10^{-1}$	65 %	$6.4 \cdot 10^{-1}$
	Exp 3	92 %	$2.1 \cdot 10^{-1}$	60 %	$6.7 \cdot 10^{-1}$
	Exp 4	90 %	$2.0 \cdot 10^{-1}$	71 %	$7.4 \cdot 10^{-1}$
Plata – Piwnik (2000)	Exp 1	78 %	$2.6 \cdot 10^{-1}$	91 %	$3.7 \cdot 10^{-1}$
	Exp 2	82 %	$4.2 \cdot 10^{-1}$	67 %	$8.6 \cdot 10^{-1}$
	Exp 3	92 %	$5.8 \cdot 10^{-1}$	61 %	$1.5 \cdot 10^{-0}$
	Exp 4	91 %	$7.1 \cdot 10^{-1}$	75 %	$2.2 \cdot 10^{-0}$
Donati – Tomesani (2004)	Exp 1	87 %	$2.3 \cdot 10^{-2}$	95 %	$5.7 \cdot 10^{-2}$
	Exp 2	87 %	$2.6 \cdot 10^{-2}$	97 %	$6.0 \cdot 10^{-2}$
	Exp 3	96 %	$2.6 \cdot 10^{-2}$	82 %	$4.3 \cdot 10^{-2}$
	Exp 4	97 %	$1.0 \cdot 10^{-3}$	74 %	$4.4 \cdot 10^{-2}$
Plata – Piwnik – Weighted (2023)	Exp 1	88 %	$7.7 \cdot 10^{-4}$	94 %	$6.8 \cdot 10^{-4}$
	Exp 2	95 %	$7.1 \cdot 10^{-4}$	98 %	$6.5 \cdot 10^{-4}$
	Exp 3	93 %	$7.0 \cdot 10^{-4}$	88 %	$6.3 \cdot 10^{-4}$
	Exp 4	97 %	$5.8 \cdot 10^{-4}$	80 %	$6.2 \cdot 10^{-4}$
Plata - Piwnik – Zener (2023)	Exp 1	45 %	$1.0 \cdot 10^{-11}$	86 %	$1.0 \cdot 10^{-15}$
	Exp 2	81 %	$5.0 \cdot 10^{-11}$	97 %	$1.5 \cdot 10^{-14}$
	Exp 3	92 %	$6.0 \cdot 10^{-10}$	85 %	$5.1 \cdot 10^{-14}$
	Exp 4	94 %	$1.6 \cdot 10^{-9}$	84 %	$1.8 \cdot 10^{-13}$

Table 5
Prediction of the bonding occurrence for each observation loci, AA2024.

Criterion	N° total loci	N° loci well predicted (AA2024)	Error (AA024)	N° loci well predicted (AA6082)	Error (AA6082)
Akeret	119	89	26 %	55	54 %
Plata - Piwnik		81	32 %	55	54 %
Donati - Tomesani		113	6 %	105	12 %
Plata - Piwnik - Weighted		115	4 %	108	9 %
Plata - Piwnik - Zener		65	46 %	86	28 %

have been identified on dedicated databases [44,45].

With the data reported in Table 7, a simple correlation analysis was performed in Excel environment and the related correlation coefficients are reported in Table 8. It is worth reminding that the closer to either −1 or 1 the coefficient values are, the stronger the relationship between the analyzed couple of items is. A coefficient value close to 1 means a strong positive relationship (one variable increases, the other increases almost proportionally). A coefficient of −1 means a strong negative relationship (one variable increases, the other decreases more or less proportionally).

Table 6
Comparison of the validation results between third-degree and linear interpolation curves, for the Plata – Piwnik – Weighted criterion.

Interpolation curve	Material	N° loci well predicted	Total observation loci	Error
Third order	AA2024	115	119	4 %
	AA7075	112	119	6 %
	AA6082	108	119	11 %
Linear	AA2024	109	119	9 %
	AA7075	113	119	6 %
	AA6082	100	119	16 %

For the slope (*m*) and y-intercept (*b*) models, TYS and SHC were selected as independent variables to build the linear model on. Actually, the correlation coefficient values were high with an absolute value very close to one. As far as the T_{start} is concerned, only the EB was selected, instead. The identified linear model equations, with the related R-squared values, are reported in Eqs. (6), (7), and (8).

As it is possible to notice in Table 8, the slope (*m*) has a negative correlation with the tensile yield strength (TYS) and the specific heat capacity (SHC), while a positive correlation was observed for the y-intercept (*b*). On other hand, the starting temperature has a negative correlation with the elongation to break (EB).

It is possible to define a generalized parametric function involving the values of the angular coefficient, constant term and starting temperature. To be more specific, for each of the considered materials, it was evaluated the equation of a straight line using the value of *m*, *b* and T_{start} calculated using the obtained correlation with TYS, SHC and EB (Eqs. (6), (7), (8)).

$$m = 4.361 \bullet 10^{-5} - 1.148 \bullet 10^{-8} \bullet TYS - 4.696 \bullet 10^{-5} \bullet SHC, R^2 = 1 \tag{6}$$

$$b = -2.089 \bullet 10^{-2} + 5 \bullet 10^{-6} \bullet TYS + 2.346 \bullet 10^{-5} \bullet SHC, R^2 = 1 \tag{7}$$

$$T_{start} = -11.311 \bullet EB + 627.48, R^2 = 0.99 \tag{8}$$

6. Parametric linear model validation

In order to test the designed parametric model, a fourth material was selected. Specifically, the AA5083 aluminum alloy was used. Please refer to Section 2.1 for the details concerning the experimental procedure. For this fourth material two process parameters configurations were investigated, namely Exp 1 and Exp 4 parameters setting of Table 2. The validation phase consisted of the following steps.

Step 1: Identifying the solid bonding map.

Step 2: Applying the iterative procedure for W^{lim} (PPW criterion) calculation in Exp 1 and Exp 4 conditions (A and B in Fig. 15).

Step 3: Collecting TYS, UTS, and EB values for the new material (AA5083).

Step 4: Building the W^{lim} linear model by applying Eqs. (6)–(8).

Step 5: Comparing the obtained prediction with that obtained with the conventional procedure (step 3).

By implementing this procedure, the obtained W^{lim} linear equation for the AA5083 material is reported in Eq. (9).

$$W^{lim} = -8.69 \cdot 10^{-7}\, T + 0.0012 \tag{9}$$

with a T_{start} equal to 426 °C.

In Fig. 15 the predicted linear model for the AA5083 material is reported together with the linear models discussed in Section 5 (Fig. 14). The W^{lim} values for the two process parameters setting are also reported (Exp 1 and Exp 4). It is worth mentioning that these values have been calculated with the automatic procedure discussed in Section 4.2. These values, therefore, serve as benchmark for assessing the accuracy of the bonding map predicted on the basis of the W^{lim} values predicted by Eq.

Table 7
List of angular coefficients (*m*), y-intercept (*b*), experimental starting temperature and thermo-mechanical properties.

	m (slope)	b (y-intercept)	T_{start} [°C]	TYS [MPa]	UTS [MPa]	EB [%]	Hv [HV]	TC [W/mm K]	SHC [J/g °C]
AA7075	−7.35E−06	0.004233	510	503	572	11	175	0.13	0.96
AA6082	−1.62E−06	0.001517	520	250	290	9	95	0.17	0.9
AA2024	−1.30E−06	0.001313	400	324	469	20	137	0.12	0.87

Table 8
Correlation values of *m*, *b* and starting temperature with the thermo-mechanical properties.

	TYS [MPa]	UTS [MPa]	EB [%]	Hv [HV]	TC [W/mm K]	SHC [J/g °C]
m (slope)	−0.944	−0.748	0.389	−0.825	0.298	−0.971
y-(intercept)	0.939	0.738	−0.403	0.817	−0.284	0.974
T_{start}	0.159	−0.228	−0.995	−0.104	0.698	0.673

(9).

It is possible to see that the predicted linear curve for the AA5083 is very close to the W^{lim} calculated in Exp 1 and Exp 4 conditions. To further explore the effectiveness of the predicted W^{lim} values, the bonding map obtained by using the W^{lim} values calculated by the iterative procedure of Section 4.2 and the W^{lim} predicted by the predicted linear model of Eq. (9) are plotted in Fig. 16 along with the experimental bonding map. It can be seen that the predicted and calculated bonding maps are very close each other and more importantly mimic the experimental map perfectly.

In this way also the second research question of the paper was effectively faced: a parametric model was set-up able to describe, with a single analytical expression, the bonding occurrence of different materials at the varying of properly selected thermo-physical characteristics.

7. Conclusions

The overall aim of this paper was to provide knowledge and tools for analyzing and predicting the bonding occurrence in Friction Stir Consolidation of aluminum alloys chips. Starting from the Plata–Piwnik–Weighted (PPW) solid bonding criterion already presented by the authors and tested for the FSC of AA7075 chips, here two more pieces of knowledge have been added.

1/The effectiveness of the PPW criterion has been proved on two more aluminum alloys, namely AA2024 and AA6082. This criterion particularly outperforms the other criteria in generalization capability. In fact, it provides the best performance also on the validation test, providing for both the proposed materials a very low error prediction (percentage of loci mistakenly predicted): namely, 6 % for AA2024 and 11 % for AA6082. These results strength the findings concerning the FSC criterion developed by the authors, making it usable for a wide range of materials (at least for aluminum alloys materials family).

2/A linear parametric model was designed to predict the W^{lim} vs Temperature curves with varying material properties. The W^{lim} vs temperature was reduced to a linear model, so that it could be modeled by knowing the slope (*m*) the y-intercept (*b*) and the activation temperature (T_{start}). Results revealed that to identify the W^{lim} curve vs temperature curve for the PPW criterion it is enough to know just the Specific Heat Capacity, the Tensile Yield Strength and the Elongation at Break of a given material.

Finally, the model was successfully tested for predicting the bonding occurrence of FSC of a further material, namely the AA5083; the predicted bonding map matched the experimental bonding map perfectly.

Further development of the present study will be addressed to enhance the applicability of such approach. Specifically, the effectiveness of the PPW criterion and the proposed parametric model will be applied to other material families such as steel and magnesium alloys.

CRediT authorship contribution statement

Riccardo Puleo: Writing – original draft, Validation, Methodology, Formal analysis, Data curation. **Abdul Latif:** Writing – original draft, Validation, Investigation, Data curation. **Giuseppe Ingarao:** Writing – review & editing, Writing – original draft, Supervision, Methodology, Conceptualization. **Livan Fratini:** Writing – review & editing, Project administration, Methodology, Funding acquisition, Conceptualization.

Declaration of competing interest

The authors disclose no actual or potential conflict of interest that could inappropriately influence, or be perceived to influence, this work.

Acknowledgements

This study was carried out within the MICS (Made in Italy – Circular and Sustainable) Extended Partnership and received funding from the European Union Next-Generation EU (PIANO NAZIONALE DI RIPRESA E RESILIENZA (PNRR) – MISSIONE 4 COMPONENTE 2, INVESTIMENTO 1.3 – D.D. 1551.11–10-2022, PE00000004).

References

[1] Ashby MF. Materials and environment. Third 2021.
[2] International Energy Agency: IEA. https://www.iea.org/.
[3] Tolio T, et al. Design, management and control of demanufacturing and remanufacturing systems. CIRP Ann Manuf Technol 2017;66(2):585–609. https://doi.org/10.1016/j.cirp.2017.05.001.
[4] Murray JW, Speidel A, Jackson-Crisp A, Smith PH, Constantin H, Clare AT. Unprocessed machining chips as a practical feedstock in directed energy deposition. Int J Mach Tool Manuf Oct. 2021;169. https://doi.org/10.1016/j.ijmachtools.2021.103803.
[5] Shahrom MS, Yusoff AR. Cyclic extrusion compression back pressure technique for hot forging process in direct recycling of aluminium 6061 machining chip. J Manuf Process Oct. 2017;29:1–9. https://doi.org/10.1016/j.jmapro.2017.07.003.
[6] Piccininni A, Cusanno A, Palumbo G, Zaheer O, Ingarao G, Fratini L. Reshaping end-of-life components by sheet hydroforming: an experimental and numerical analysis. J Mater Process Technol Aug. 2022;306. https://doi.org/10.1016/j.jmatprotec.2022.117650.
[7] Baffari D, Reynolds AP, Masnata A, Fratini L, Ingarao G. Friction stir extrusion to recycle aluminum alloys scraps: energy efficiency characterization. J Manuf Process Jul. 2019;43:63–9. https://doi.org/10.1016/j.jmapro.2019.03.049.
[8] Wan B, Chen W, Lu T, Liu F, Jiang Z, Mao M. Review of solid state recycling of aluminum chips. Resources, Conservation and Recycling 2017;125:37–47. https://doi.org/10.1016/j.resconrec.2017.06.004. Elsevier B.V.
[9] Chiba R, Yoshimura M. Solid-state recycling of aluminium alloy swarf into c-channel by hot extrusion. J Manuf Process Jan. 2015;17:1–8. https://doi.org/10.1016/j.jmapro.2014.10.002.
[10] Selvaggio A, Erman Tekkaya A. Identification of factors influencing the quality of extruded profiles using aluminum recyclate-based billets. Manuf Lett Aug. 2023;35:1326–35. https://doi.org/10.1016/J.MFGLET.2023.08.076.
[11] Sadasivan N, Balasubramanian M, Rameshbapu BR. A comprehensive review on equal channel angular pressing of bulk metal and sheet metal process methodology and its varied applications. J Manuf Process Nov. 2020;59:698–726. https://doi.org/10.1016/J.JMAPRO.2020.10.032.
[12] Paraskevas D, Dadbakhsh S, Vleugels J, Vanmeensel K, Dewulf W, Duflou JR. Solid state recycling of pure Mg and AZ31 Mg machining chips via spark plasma

sintering. Mater Des Nov. 2016;109:520–9. https://doi.org/10.1016/j.matdes.2016.07.082.
[13] Paraskevas D, Vanmeensel K, Vleugels J, Dewulf W, Deng Y, Duflou JR. Spark plasma sintering as a solid-state recycling technique: the case of aluminum alloy scrap consolidation. Materials 2014;7(8):5664–87. https://doi.org/10.3390/ma7085664.
[14] Koch A, Bonhage M, Teschke M, Luecker L, Behrens BA, Walther F. Electrical resistance-based fatigue assessment and capability prediction of extrudates from recycled field-assisted sintered EN AW-6082 aluminium chips. Mater Charact Nov. 2020;169. https://doi.org/10.1016/j.matchar.2020.110644.
[15] Jarrell AW, Strauss AM. Applying torque based control to friction stir extrusion. J Manuf Process Aug. 2022;80:382–96. https://doi.org/10.1016/j.jmapro.2022.06.002.
[16] Baffari D, Reynolds AP, Li X, Fratini L. Influence of processing parameters and initial temper on friction stir extrusion of 2050 aluminum alloy. J Manuf Process Aug. 2017;28:319–25. https://doi.org/10.1016/j.jmapro.2017.06.013.
[17] Topolski K. Relationship of microstructure and properties of high-purity titanium manufactured by unconventional method of chips recycling. J Manuf Process May 2022;77:426–38. https://doi.org/10.1016/j.jmapro.2022.03.011.
[18] Taysom BS, et al. Shear assisted processing and extrusion of enhanced strength aluminum alloy tubing. Int J Mach Tool Manuf Oct. 2021;169. https://doi.org/10.1016/j.ijmachtools.2021.103798.
[19] Whalen S, et al. Porthole die extrusion of aluminum 6063 industrial scrap by shear assisted processing and extrusion. Manuf Lett Jul. 2023;36:52–6. https://doi.org/10.1016/j.mfglet.2023.01.005.
[20] Borgert T, Milaege D, Schweizer S, Homberg W, Schaper M, Tröster T. Potentials of a friction-induced recycling process to improve resource and energy efficiency in manufacturing technology. International Journal of Material Forming Nov. 2023;16(6). https://doi.org/10.1007/s12289-023-01785-w.
[21] Li X, Baffari D, Reynolds AP. Friction stir consolidation of aluminum machining chips. Int J Adv Manuf Technol Feb. 2018;94(5–8):2031–42. https://doi.org/10.1007/s00170-017-1016-4.
[22] W. Tang and A. P. Reynolds, “Friction Consolidation of Aluminum Chips.”.
[23] Buffa G, Baffari D, Ingarao G, Fratini L. Uncovering technological and environmental potentials of aluminum alloy scraps recycling through friction stir consolidation. International Journal of Precision Engineering and Manufacturing - Green Technology Sep. 2020;7(5):955–64. https://doi.org/10.1007/s40684-019-00159-5.
[24] Latif A, Ingarao G, Gucciardi M, Fratini L. A novel approach to enhance mechanical properties during recycling of aluminum alloy scrap through friction stir consolidation. Int J Adv Manuf Technol Mar. 2022;119(3–4):1989–2005. https://doi.org/10.1007/s00170-021-08346-y.
[25] Akeret R. Extrusion welds-quality aspects are now center stage. In: Proceedings of the 5th international aluminum extrusion technology seminar; 1992. p. 319–36.
[26] Plata MPJ. Theoretical and experimental analysis of seam weld formation in hot extrusion of aluminium alloys. In: Proceedings of the 7th international aluminium extrusion seminar; 2000. p. 205–12.
[27] Donati L, Tomesani L. The prediction of seam welds quality in aluminum extrusion. J Mater Process Technol Nov. 2004;153–154(1–3):366–73. https://doi.org/10.1016/j.jmatprotec.2004.04.215.
[28] Ceretti E, Fratini L, Gagliardi F, Giardini C. A new approach to study material bonding in extrusion porthole dies. CIRP Ann Manuf Technol 2009;58(1):259–62. https://doi.org/10.1016/j.cirp.2009.03.010.
[29] Bay N. Cold pressure welding—the mechanisms governing bonding. 1979.
[30] Cooper DR, Allwood JM. The influence of deformation conditions in solid-state aluminium welding processes on the resulting weld strength. J Mater Process Technol 2014;214(11):2576–92. https://doi.org/10.1016/j.jmatprotec.2014.04.018.
[31] Oberhausen G, Cooper DR. Modeling the strength of aluminum extrusion transverse welds using the film theory of solid-state welding. J Mater Process Technol Mar. 2024;324. https://doi.org/10.1016/j.jmatprotec.2023.118254.
[32] Kolpak F, Schulze A, Dahnke C, Tekkaya AE. Predicting weld-quality in direct hot extrusion of aluminium chips. J Mater Process Technol Dec. 2019;274. https://doi.org/10.1016/j.jmatprotec.2019.116294.
[33] Yu J, Zhao G, Chen L. Analysis of longitudinal weld seam defects and investigation of solid-state bonding criteria in porthole die extrusion process of aluminum alloy profiles. J Mater Process Technol Nov. 2016;237:31–47. https://doi.org/10.1016/j.jmatprotec.2016.05.024.
[34] Güley V, Güzel A, Jäger A, Ben Khalifa N, Tekkaya AE, Misiolek WZ. Effect of die design on the welding quality during solid state recycling of AA6060 chips by hot extrusion. Mater Sci Eng A Jul. 2013;574:163–75. https://doi.org/10.1016/j.msea.2013.03.010.
[35] Baffari D, Buffa G, Fratini L. A numerical model for wire integrity prediction in friction stir extrusion of magnesium alloys. J Mater Process Technol Sep. 2017;247:1–10. https://doi.org/10.1016/j.jmatprotec.2017.04.007.
[36] Puleo R, Latif A, Ingarao G, Di Lorenzo R, Fratini L. Solid bonding criteria design for aluminum chips recycling through friction stir consolidation. J Mater Process Technol 2023;319. https://doi.org/10.1016/j.jmatprotec.2023.118080.
[37] Raabe D, et al. Making sustainable aluminum by recycling scrap: the science of ‘dirty’ alloys. Progress in Materials Science 2022;128. https://doi.org/10.1016/j.pmatsci.2022.100947. Elsevier Ltd, Jul. 01.
[38] Latif A, Gucciardi M, Ingarao G, Fratini L. Outlining the limits of friction stir consolidation as used as an aluminum alloys recycling approach. In: Smart innovation, systems and technologies. Springer Science and Business Media Deutschland GmbH; 2022. p. 169–80. https://doi.org/10.1007/978-981-16-6128-0_17.
[39] Shima S OM. Plasticity theory for porous metals. Int J Mech Sci 1976;18:286–91.
[40] Buffa G, Pellegrino S, Fratini L. Analytical bonding criteria for joint integrity prediction in friction stir welding of aluminum alloys. J Mater Process Technol 2014;214(10):2102–11. https://doi.org/10.1016/j.jmatprotec.2014.02.014.
[41] Huda Z, Zaharinie T. Kinetics of grain growth in 2024-T3: an aerospace aluminum alloy. J Alloys Compd Jun. 2009;478(1–2):128–32. https://doi.org/10.1016/j.jallcom.2008.11.071.
[42] El-Danaf EA, Almajid AA, Soliman MS. Hot deformation of AA6082-T4 aluminum alloy. J Mater Sci Sep. 2008;43(18):6324–30. https://doi.org/10.1007/s10853-008-2895-4.
[43] Mcqueen HJ, Fry E, Belling J. Comparative constitutive constants for hot working of Al-4.4Mg-0.7Mn (AA5083). ASM International; 2001.
[44] GRANTA EduPack. https://www.grantadesign.com/it/education/ces-edupack/.
[45] MatWeb. https://www.matweb.com/.